Am J Cancer Res 2024;14(5):2643-2660
www.ajcr.us /ISSN:2156-6976/ajcr0155464

*Original Article*

# MicroRNA 421 induces the formation of high-invasive cell subsets of ovarian cancer from low-invasive cell subsets mediated by exosomes by activating the PI3K/AKT pathway

Qianlong Meng[1,2*], Wei Zheng[1*], Ruili Jiao[3], Ran Cui[4], Yunhan Deng[5], Ruizhen Liu[5], Jing Wang[6,7], Huimin Bai[1]

*[1]Department of Gynecology, Fuxing Hospital, Capital Medical University, Beijing, China; [2]Department of Diagnostics of Clinical Laboratory, Zhejiang Hospital, Hangzhou, Zhejiang, China; [3]Department of Obstetrics and Gynecology, Beijing Chaoyang District Maternal and Child Health Hospital, Beijing, China; [4]Department of Obstetrics and Gynecology, Peking University First Hospital, Beijing, China; [5]Department of Obstetrics and Gynecology, Beijing Chaoyang Hospital, Capital Medical University, Beijing, China; [6]Beijing Key Laboratory of Mental Disorders, National Clinical Research Center for Mental Disorders and National Center for Mental Disorders, Beijing Anding Hospital, Capital Medical University, Beijing, China; [7]Advanced Innovation Center for Human Brain Protection, Capital Medical University, Beijing, China. [*]Equal contributors.*

Received January 15, 2024; Accepted May 15, 2024; Epub May 15, 2024; Published May 30, 2024

**Abstract:** Intratumoral heterogeneity (ITH) results in treatment failure in ovarian cancer (OC). Exosomes are related to the formation of a heterogeneous tumor microenvironment, and microRNAs play a crucial role in the progression of OC. Therefore, we aimed to explore the effect of exosomes and microRNA 421 (miR-421), which is mediated by exosomes, on ITH and the diagnosis of OC. Exosomes derived from A2780 cells with the highest (AHC) or lowest (ALC) invasive/migratory capacity cells (AHE/ALE) were extracted by differential centrifugation. We conducted a series of experiments to verify the role of AHE and miR-421 in promoting the transformation of low-invasive cells to high-invasive cells by regulating the PI3K/AKT pathway, and we also measured the levels of CA125 in serum exosomes. The results of assays showed that the AHE and miR-421, mediated by exosomes, significantly increased the malignancy of ALC cells by activating the PI3K/AKT pathway. The expression of miR-421 was significantly increased in the serum exosomes derived from high-grade serous ovarian cancer (HGSOC) patients. Our findings indicate that MiR-421, mediated by exosomes, could induce the transformation of highly invasive cell subpopulations from subpopulations of OC cells with low invasive potential by activating the PI3K/AKT signaling pathway.

**Keywords:** Ovarian cancer, tumor heterogeneity, exosomes, PI3K/AKT pathway, miR-421

## Introduction

OC is the third most common gynecologic malignancy worldwide and has the highest mortality rate among these cancers. Heterogeneity is a common phenomenon of parental tumor cell lines, and highly metastatic tumor cell variants preexist in parental tumor cell populations. ITH has resulted in treatment failure in many human malignancies. The tumor microenvironment (TME) of ovarian cancer is complex and unique. The cellular composition of TME varies among different tissues in the human body. The characteristic of HGSOC is the high heterogeneity of TME within the patient [1]. The extracellular matrix (ECM) also affects various functions of tumor cells, including proliferation, survival, invasion and migration, stem cells, and resistance to treatment. ECM mediates the latter by activating anti-Kapoptotic and stem cell signaling pathways, serving as a physical barrier for drugs [2-4].

Our previously published studies demonstrated that OC is also a kind of heterogeneous disease [5]. Exosomes are extracellular vesicles with diameters of 50-140 nm that can carry small molecules, such as proteins, and

https://doi.org/10.62347/UHEY7375

RNAs. Exosomes are related to the formation of a tumor heterogeneous microenvironment. One of our previous studies revealed that exosomes derived from OC cells contain specific proteins related to OC genesis and metastasis. OC exosomes promote the formation of pre-metastatic niches through immune suppression, angiogenesis, stromal cell remodeling, and oncogenic reprogramming [6, 7]. The study has found that serum exosomes from ovarian cancer patients contribute to the migration of cancer cells and may serve as important diagnostic and prognostic biomarkers for ovarian cancer [8].

However, there are interactions between miRNAs and regulatory proteins in TME, further research is needed to confirm whether the regulatory mechanisms involved are related to tumor type, stage, and heterogeneity. In addition, the recognition process between miRNAs and receptor cells, as well as the composition of miRNA delivery systems, the transport and transmission of miRNAs in the exosomes secreted by cells in TME, and their specific roles in promoting tumorigenesis and metastasis, have not been fully elucidated. This requires more in-depth research on the use of miRNAs contained in exosomes and their therapeutic applications [9, 10].

The phosphoinositide 3-kinase (PI3K)/AKT pathway has been reported as a frequently altered signaling pathway in OC. However, PI3K inhibitors alone do not significantly inhibit the proliferation of primary OC cells, and various inhibitors of the PI3K pathway have shown little success in clinical trials. Recent studies revealed that exosomes could promote tumor progression by mediating the PI3K/AKT pathway. Whether exosomes can mediate the PI3K/AKT pathway to promote the progression of OC has not been reported. To explore the molecular mechanism of the development of OC heterogeneity, we established a relevant cell research model [5, 11]. Single-cell subclones with the strongest and weakest invasion/migration ability (renamed AHC and ALC, respectively) were isolated and screened from the human OC cell line A2780 using a limited dilution method. The results of RNA sequencing and bioinformatics analysis suggested that aberrant activation of the PI3K/AKT pathway was associated with the formation of highly invasive cell subclones in OC. Based on research results, we hypothesized that changes in the heterogeneity of OC cells can be mediated by exosomes, which can also alter the malignancy of OC cells. MicroRNAs in exosomes play important regulatory roles. The regulatory effect of exosomes and their contained microRNAs on OC heterogeneity is achieved by affecting the PI3K/AKT pathway.

In this study, we investigated the effect of AHE on the heterogeneity of ovarian cancer cells, and the candidate differentially expressed microRNAs (DEMs) with a potential regulatory effect on the PI3K/AKT pathway were identified by bioinformatics analysis. The association between the expression level of the candidate DEMs and the clinicopathological characteristics of OC patients was also explored. This study identified the presence of the DEMs in different OC exosomes, and the DEMs are the cause of heterogeneity in ovarian cancer. The DEMs can not only serve as diagnostic markers for OC but also be used for pathological classification and prognosis assessment of OC. This study provides a new diagnostic direction for early detection of OC and provides valuable preclinical evidence that could guide individualized molecular targeted therapy for OC.

## Materials and methods

### *Ethics approval*

The study was conducted with the understanding and written informed consent of each patient or their relatives. The experimental protocol was established according to the ethical standards and the Declaration of Helsinki. The study was approved by the Human Ethics Committee of Beijing Chaoyang Hospital, Capital Medical University.

### *Cell culture and transfection*

The subclones of A2780 (CVCL_0134) cells obtained from the Basic Research Institute of Peking Union Medical College Hospital with the highest or lowest invasive/migratory capacity (AHC and ALC, respectively) were isolated and established through a limiting dilution methodology, as we described previously [11, 12]. AHC/ALC cells were cultured in RPMI-1640 medium (Corning) containing 10% fetal bovine serum and antibiotics of 1% penicillin-strepto-

mycin solution at 37°C in a humidified atmosphere incubator with 5% $CO_2$. The candidate DEM mimic/inhibitor (100 uM) and negative controls (100 uM) were transfected into AHC cells using the RiboFECT CP Transfection Kit (Ruibo Biology Co., Ltd.). All experiments were performed with mycoplasma-free cells in this paper.

*Cell line authentication process*

All cell lines have been authenticated in the past three years. Take an appropriate amount of A2780 cells and use the TIAAmp Genomic DNA Kit to extract DNA. 20 STR loci and gender identification loci were amplified using the MicroreaderTM21 ID system, and the PCR products were detected using the GenReader 7010 gene analyzer. The detection results were analyzed using GeneMapper Software6 software (Applied Biosystems) and compared with the ExPASy database. The STR typing results of the cell line DNA showed that no human cell cross-contamination was found in the A2780 cell line.

*CCK-8 proliferation assay*

Cells were seeded into 96-well plates at a density of $2\times10^3$ cells and cultured with medium containing 10% FBS (Corning) for 24 h, 48 h, 72 h, 96 h, and 120 h, respectively. At 72 h and 120 h, the culture medium was changed. Cell proliferation was by CCK8 solution reagent (KeyGEN BioTECH) and assessed according to the optical density (OD) detected by a 96-well plate reader (BIO-RAD Microplate Reader). All experiments were repeated three times with six replicate wells.

The concentration of exosomes derived from AHC (AHE) co-cultured with ALC cells was 80 μg/mL in the experiment groups and control groups used the same volume of PBS. The EdU assay, wound healing assay, matrigel migration/invasion assay and cell immunofluorescence assay all adapted the above AHE concentration.

*EdU assay*

An EdU kit (RiboBio) was used according to the instructions. The results were observed and imaged with a fluorescence microscope (Leica DM2500). The experiment was performed three times.

*Colony formation assay*

Cells were plated into six-well plates (Corning) (500 cells per well) and cultured for 14 days until visible cell colonies appeared. The colonies were fixed with 4% PFA and stained with 0.1% crystal violet. The number of colonies was counted and compared.

*Wound healing assay*

ALC and AHC cells were cultured in 6-well plates until the cell density reached 90%. The cell monolayers were wounded with a 200 μl pipette tip to scratch a gap in the plates. The plates were gently washed with PBS three times to remove the floating cells, and the culture medium was replaced with a serum-free medium. The wound closure area at the first scratch (0 h) and after 24 h were observed and photographed by microscopy with Leica software. The healing area was measured using ImageJ software.

*Matrigel migration/invasion assay*

For the migration assay, ALC and AHC cells were harvested and resuspended in a serum-free medium. Then, the cells ($3\times10^6$ cells/ml) were seeded into the upper chamber. RPMI-1640 medium with 20% FBS was added to the lower chamber. After incubation for 24 h, the invaded cells were fixed with 4% PFA, washed with PBS, and stained with 0.5% crystal violet. For the invasion assay, the chambers were coated with diluted Matrigel. Then, cells were suspended in an RPMI-1640-only medium and loaded in the upper chambers. The following steps were consistent with those of the migration assay. The migratory or invaded cells were photographed and counted under a microscope.

*Cell immunofluorescence assay*

Cells were cultured on poly-L-lysine-coated coverslips ($8\times10^4$ cells per well) in 24-well plates. After being cultured for 24 h, cells were fixed with 4% PFA at room temperature for 15 min and then permeabilized with 0.1% Triton X-100 for 10 min. BSA (1%) in PBS was used to block nonspecific binding for 1 h. Then, the cells were treated with anti-E cadherin (CST), anti-N cadherin (CST), and anti-Vimentin antibodies (CST) at 4°C overnight. The cells were stained with

goat anti-rabbit secondary antibody (Invitrogen) at room temperature for 2 h in a dark box and then stained with DAPI for 10 min. The fluorescence of the cells was visualized by fluorescence microscopy.

*Western blot (WB) assay*

The cells were lysed in ice-cold radioimmunoprecipitation assay (RIPA) lysis buffer with a 1% protease inhibitor. The BCA assay kit (Thermo) was used to determine the total protein concentration. Equal amounts of protein were separated using SDS-PAGE gel and transferred onto a nitrocellulose (NC) membrane. Then, the membrane was blocked with 5% bovine serum albumin (BSA) dissolved in Tris-buffered saline with Tween-20 (TBST) for 1.5 h at room temperature and incubated with primary antibodies specific to protein at 4°C overnight. The following antibodies against proteins were used: E-cadherin (CST, #3195C), N-cadherin (CST, #13116), vimentin (CST, #5741), p-PI3K (CST, #17366S), PI3K (CST, #4255), p-AKT (CST, #4060), AKT (CST, #4685S) and GAPDH (Abcam, ab8245). After being washed in TBST buffer three times, the membrane was incubated with horseradish peroxidase-conjugated goat anti-rabbit antibody (Beyotime Biotechnology; 1:5000) or anti-mouse antibody (Beyotime Biotechnology; 1:5000) secondary antibodies for 1.5 h and then washed with TBST buffer three times again. Finally, the protein bands were scanned with an enhanced chemiluminescence kit on a Chemiluminescence Imaging System (Minichemi) with Image Lab software.

*Exosomes isolation*

Cells were cultured at approximately 60-70% density and washed twice with PBS to eliminate the interference of exosomes in serum. Then, the medium from each culture plate was replaced by 10% exosomes-depleted FBS, which was centrifuged at 110000 × g and 4°C overnight (> 12 h) [13, 14]. Extraction of exosomes by differential centrifugation. The Pierce TM BCA Protein Assay Kit was used to quantify the protein concentration.

*Transmission electron microscopy (TEM)*

The morphology and size of exosomes were observed by TEM using negative staining with copper mesh, as described previously [13, 15]. Exosome precipitates were resuspended using 50-100 μL 2% PFA, loaded onto a formvar-carbon-coated grid, and incubated for 20 min. After being washed twice with PBS, the grid was refixed with 1% glutaraldehyde for 5 min. The grid was washed 8 times using double-distilled water. The grid was first contrasted in a solution of uranyl oxalate, pH 7.0, then determined and embedded in a mixture of 4% uranyl acetate and 2% methylcellulose in 100 μl/900 μl. The grid was dried in air for 5-10 min. The grid was observed under an electron microscope at 80 kV.

*Nanoparticle tracking analysis (NTA)*

NTA measured the concentration and size distribution of exosomes released from AHC and ALC cell. The samples were loaded into the NanoSight NS300 instrument (Malvern, UK) to analyze the size and concentration of exosomes.

*Exosome labeling and uptake assay*

The PKH67 Green Fluorescent Cell Linker Mini Kit (Sigma) was used to label AHE. The procedure was conducted according to the instructions. Phallotoxins (Beyotime Biotechnology) were used to label F-actin to show cell morphology.

*Quantitative miRNA analysis and identification of candidate DEMs*

Total RNA was extracted from ALE and AHE and quantitatively determined by BGI company using BGISEQ-500 sequencing. DEMs were defined by default as those with false discovery rates (FDR) ≤ 0.001 and a fold change of more than 2. Multiple databases, including TargetScan, miRanda, and RNAhybrid, were used to predict the target genes of the DEMs. The Kyoto Encyclopedia of Genes and Genomes (KEGG) database was used to predict the biological function of the target genes. The candidate DEMs with a potential regulatory effect on the PI3K/AKT pathway were selected for further evaluation.

*Quantitative real-time PCR (qRT-PCR)*

Total RNA was extracted using TRIzol reagent (Invitrogen). The RNA was reverse-transcribed

to cDNA using the Mir-X miRNA First-Strand Synthesis Kit (Takara, 638315). U6, a small nuclear RNA (snRNA), was used as an internal control to normalize the cell miRNA results. Cel-miR-39-3p (miRB0000010, RiboBio), the standard RNA, was spiked as an exogenous control to normalize exosomes and serum sample miRNA results. miRNA expression was detected by qRT-PCR using the Mir-X miRNA qRT-PCR TB Green® Kit (Takara, 638314) on a 7500 Real-time PCR System (Applied Biosystems). The $2^{-\Delta\Delta}$ Ct method was used to analyze the differences in relative expression levels between groups.

*Patient samples*

Serum samples from patients with HGSOC (high-grade serous ovarian carcinoma) and benign ovarian tumors were collected in sterile tubes. Patient clinicopathological characteristics, such as age, menopause state, International Federation of Obstetrics and Gynecology (FIGO) stage, tumor node metastasis (TNM) stage, histologic grade, tumor size, differentiation degree, lymph node metastasis, and pretreatment serum CA125 levels, were collected. Patient serum was centrifuged at 12000 × g for 30 min at 4°C to remove cellular fractions. The separated serum was aliquoted and stored at -80°C until further processing. Repeated defrosting was avoided when possible. The expression of the candidate DEMs in serum exosomes was determined by qRT-PCR.

*Statistical analysis*

All statistical analyses were performed using the statistical software SPSS version 22.0 and GraphPad Prism software (8.0). The statistical significance of the results was determined using Student's t-test between the experimental group and control group. Statistical differences in exosomal miRNA expressions between HGSOC (46 cases) and benign tumors (12 cases) were calculated using two-tailed Student's t-test. The correlations of serum levels of exosomal miRNAs and clinical pathological characteristics of patients were evaluated by the Spearman rho test. ROC curve is an effective tool for the comprehensive and accurate evaluation of diagnostic experiments [16]. The diagnostic power of the exosomal miRNAs was analyzed by ROC curves with corresponding statistics [17]. The cutoff values for the relative expression levels of miRNAs and the clinical markers alone and in combination were determined by the Youden index from the ROC curves. Differences were considered significant when $P < 0.05$.

## Result

*Reidentification of the distinct biological characteristics of AHC and ALC*

The CCK-8 assay growth curves showed that the AHC cell growth rate increased significantly faster than the ALC cell growth rate ($P < 0.001$, **Figure 1A**). The EdU assay and colony formation assay demonstrated that the AHC cells had a significantly higher percentage of proliferating cells (80.06 ± 3.95% vs. 46.44 ± 3.85%, $P < 0.0001$; **Figure 1B**) than ALC and more number of colonies (55.93 ± 4.63% vs. 29.47 ± 1.88%, $P < 0.005$; **Figure 1C**) than ALC. The wound healing rate of AHC cells was significantly higher than that of ALC (44.47 ± 3.34% vs. 23.97 ± 3.61%, $P < 0.001$; **Figure 1D**). AHC cell demonstrated a significantly stronger ability to invade (82.89 ± 5.86 vs. 32.4 ± 6.28, $P < 0.0001$; **Figure 1E**) and migrate (665.89 ± 24.19 vs. 158.67 ± 9.12, $P < 0.0001$; **Figure 1E**) than ALC cell. Immunofluorescence staining showed that the expression levels of N-cadherin (0.478 ± 0.097 vs. 0.165 ± 0.032, $P = 0.024$; **Figure 1F**) and vimentin (1.020 ± 0.126 vs. 0.353 ± 0.020, $P < 0.005$; **Figure 1F**) were significantly higher in AHC than in ALC. The results of WB assays confirmed the immunofluorescence staining results (**Figure 1G**), and the results also indicated that the PI3K/AKT pathway in AHC was significantly activated compared to that in ALC (**Figure 1H**). In summary, the EMT capacity of AHC cells was significantly higher than that of ALC, and the PI3K/AKT pathway was activated in AHC. Thus, AHC displayed significantly higher invasive and migratory capacities and greater anchorage-independent growth viability than ALC. AHC/ALC is still the ideal cell model for research on the tumor heterogeneity of OC and could be used for further analysis.

*Isolation and identification of exosomes derived from ALC and AHC*

Exosomes were isolated from the supernatant of AHC cells (AHE) and ALC (ALE) by gradient centrifugation (**Figure 2A**). TEM showed that exosomes had a typical cup-shaped morphology between 50 nm and 140 nm (**Figure 2B**).

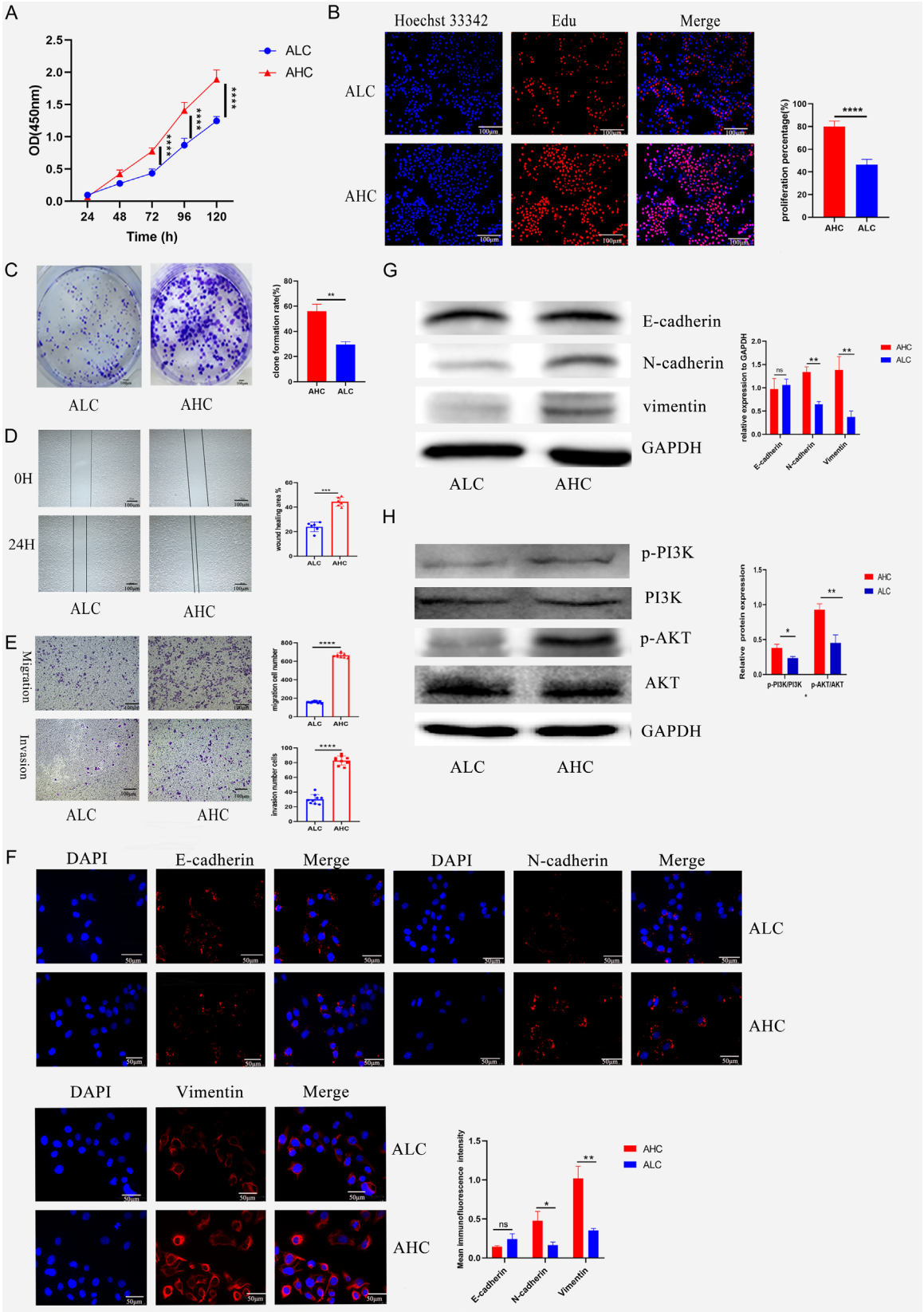


**Figure 1.** Reidentification of the distinct biological characteristics of AHC and ALC. A. CCK-8 assay detected that the proliferation ability of AHC is significantly higher than that of ALC. B. EDU assay detected that AHC has a higher pro-

liferation percentage than ALC (80.06 ± 3.95% vs. 46.44 ± 3.85%, P < 0.0001). C. Colony formation assay detected the efficiency of clone formation between AHC and ALC after being cultured for 14 days. D. Wound healing assay showed that AHC had significantly higher migration area percentages than ALC (44.47 ± 3.34% vs. 23.97 ± 3.61%, P < 0.001) after 24 hours of cultivation. E. AHC had higher ability of migration (665.89 ± 24.19 vs. 158.67 ± 9.12, P < 0.0001) and invasion (82.89 ± 5.86 vs. 32.4 ± 6.28, P < 0.0001) than ALC by Transwell Matrigel invasion/migration assay. F. Immunofluorescence staining revealed that the experiment revealed that the expression levels of N-cadherin (0.478 ± 0.097 vs. 0.165 ± 0.032, P = 0.024) and Vimentin (1.020 ± 0.126 vs. 0.353 ± 0.020, P < 0.005) in AHC were significantly higher than those in ALC. The expression level of E-cadherin (0.973 ± 0.187 vs. 1.063 ± 0.103, P = 0.584) is slightly higher in ALC than in AHC. G. The WB results of E-cadherin, N-cadherin, and Vimentin confirmed the immunofluorescence staining. H. WB assay showed that the expression level of p-PI3K/PI3K (0.382 ± 0.053 vs. 0.234 ± 0.023, P < 0.05) and p-AKT/AKT (1.037 ± 0.095 vs. 0.463 ± 0.103, P < 0.005) in AHC were significantly higher than that in ALC. The data were presented as the mean ± SD. *P < 0.05, **P < 0.005, ***P < 0.001, ****P < 0.0001. The scale bar equals 50 or 100 μm as indicated in the graph.

The NTA results showed that the average diameters of isolated exosomes from AHC and ALC were 102.7 nm and 121.8 nm, respectively. The average number of nanoparticles/ml was $7.0\times10^7$ and $4.3\times10^7$, respectively (**Figure 2C**). The expression of CD9, CD63, and Alix was positive, and calnexin was absent in the exosomes (**Figure 2D**). Exosome labeling and uptake assays revealed that AHE labeled with PKH67 could be dispersed in the cytoplasm of ALC cells (**Figure 2E**).

*The effect of AHE on the biological functions of ALC*

CCK-8 and EdU assays consistently showed that the proliferative activity of ALC was significantly enhanced after AHE coculturing (P < 0.001; **Figure 2F**, **2I**). Wound-healing assays (P < 0.005; **Figure 2G**), colony formation assay (432.51 ± 23.54 vs. 575.54 ± 36.57, P < 0.05; **Figure 2H**), and Matrigel migration/invasion assays (P < 0.001; **Figure 2J**) revealed that AHE could significantly promote the migration and invasion of ALC. The WB assay showed slightly elevated expression of E-cadherin. The expression of N-cadherin and vimentin after incubation with AHE was significantly increased, indicating that AHE could induce ALC to undergo EMT (P < 0.001; **Figure 2K**). In addition, the extent of elevation of N-cadherin and vimentin expression in ALC was dependent on the concentration of AHE, and these values were positively correlated (**Figure 2L**).

*The effect of AHE on the activity of the PI3K/AKT pathway in ALC cells*

The expression of p-PI3K and p-AKT was significantly elevated in ALC cells after incubation with AHE (**Figure 2K**; P < 0.005). The levels of p-PI3K and p-AKT increased with the concentration of AHE (**Figure 2L**; P < 0.005). The WB assay revealed that the optimal inhibitory concentration of LY294002 was 15 μM (**Figure 2M**), and LY294002 attenuated the increase in p-PI3K and p-AKT levels after treatment with AHE (**Figure 2N**; P < 0.001).

*Screening and analysis of DEMs between ALE and AHE*

The results of quantitative miRNA sequencing showed that a total of 3236 miRNAs were detected in the total RNA of ALE/AHE, including 1617 known and 1619 novel miRNAs. According to thresholds of FDR ≤ 0.001 and fold change > 2, a total of 1667 DEMs (939 upregulated and 728 downregulated miRNAs) were identified in the AHE compared to the ALE (**Figure 3A**). The Venn diagram of targeted gene prediction using three online miRNA target analysis websites (TargetScan, miRanda, and RNAhybrid) showed that 1094299 genes were the target genes of the DEMs (**Figure 3B**). KEGG analysis showed that a total of 33 DEMs had a potential regulatory effect on the PI3K/AKT pathway (**Figure 3C**; Table S1). Ten DEMs had a potential role in tumorigenesis and progression based on reports in the literature (**Figure 3D**; **Table 1**). The qRT-PCR results confirmed that eight of the DEMs (miR-378b, miR-1910-3p, miR-21-3p, miR-421, miR-221-3p, miR-324-3p, miR-3065-3p, and miR-222-3p) were significantly elevated in AHE compared with ALE, consistent with the results of miRNA sequencing (**Figure 3E**, **3F**). These eight DEMs were identified as candidate DEMs for further analysis.

*The relationship between the expression levels of the candidate DEMs and the clinicopathological characteristics of OC patients*

Serum samples of 58 patients with HGSOC (46 cases) and benign tumors (12 cases) were col-

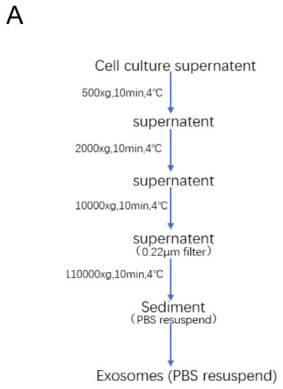


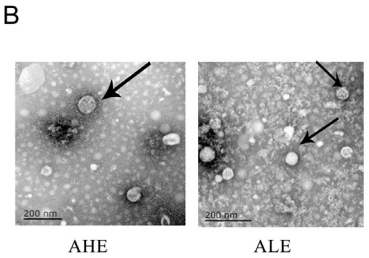


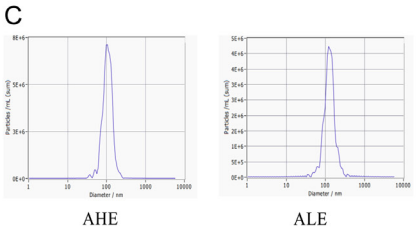


| sample | dilution ratio | concernation (particles/mL) | average diameter (nm) |
|---|---|---|---|
| AHE | 1600 | 7.0E+07 | 102.7 |
| ALE | 1600 | 4.3E+07 | 121.8 |

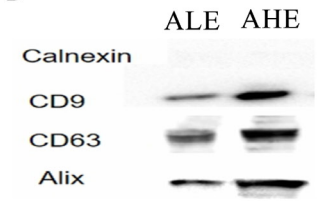


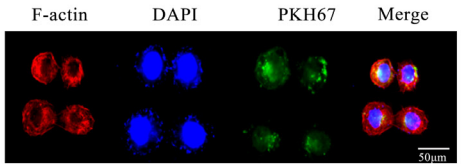


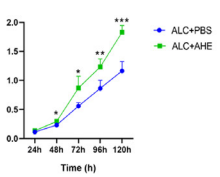


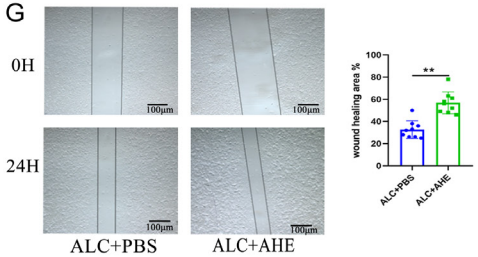


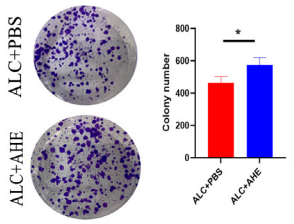


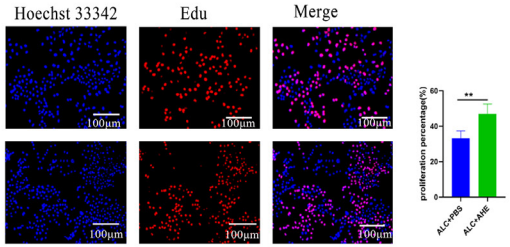


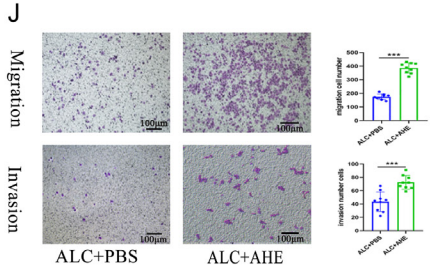


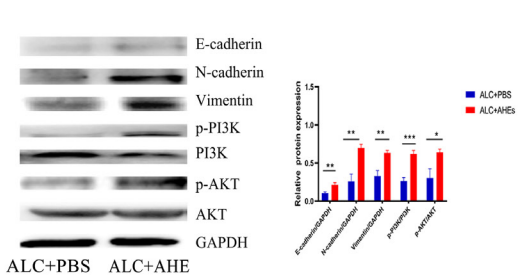


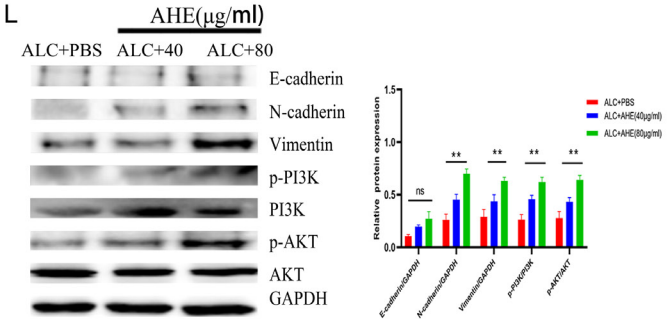


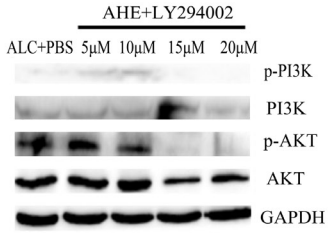


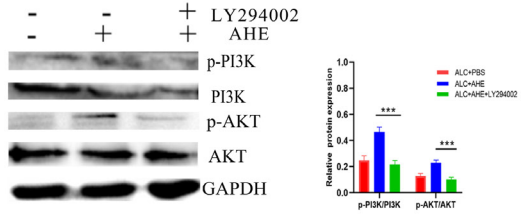

**Figure 2.** Isolation and identification of exosomes and the effect of AHE on ALC. (A) Experimental steps of the Differential centrifugation method. (B, C) TEM and NTA were used to identify the morphology and size of exosomes. (D) WB assay was used to detect the extracellular surface markers CD9, CD63, and Alix. (E) Immunofluorescence assay to assess the ALC uptake of AHE. (F) CCK-8 assay, (G) Wound healing assay, (H) Colony formation assay (432.51 ± 23.54 vs. 575.54 ± 36.57, P < 0.05), (I) EDU assay and (J) Transwell Matrigel invasion/migration assay showed that the ability of proliferation, migration, invasion of ALC treated with AHE was significantly higher than ALC treated with PBS. (K) The protein expression of E-cadherin, N-cadherin, and Vimentin in ALC treated with AHE was higher than in ALC treated with PBS. Similarly, the WB assay showed that the expression of p-PI3K/PI3K and p-AKT/AKT were significantly higher than in ALC treated with PBS. (L) The promoting effect of AHE on EMT and the activation of the PI3K/AKT pathway were concentration-dependent in ALC. (M) WB assay was used to determine the optimal action concentration of LY294002 in ALC by detecting the protein expression of the PI3K/AKT signaling pathway. (N) The activation of the PI3K/AKT pathway in ALC by AHE can be inhibited by LY294002. GAPDH was used as a loading control. The data were presented as the mean ± SD. *P < 0.05, **P < 0.005, ***P < 0.001, ****P < 0.0001. The scale bar equals 50 or 100 μm as indicated in the graph.

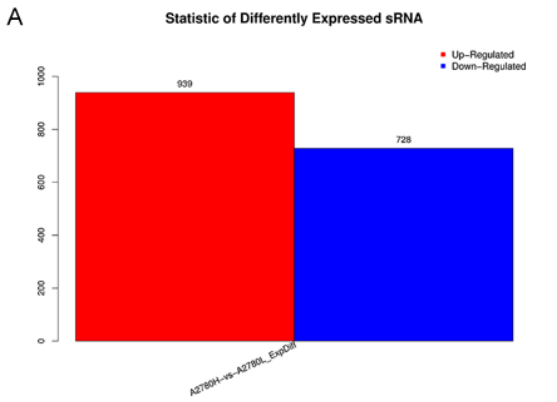


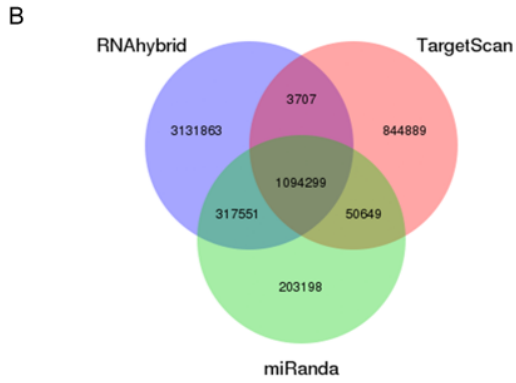


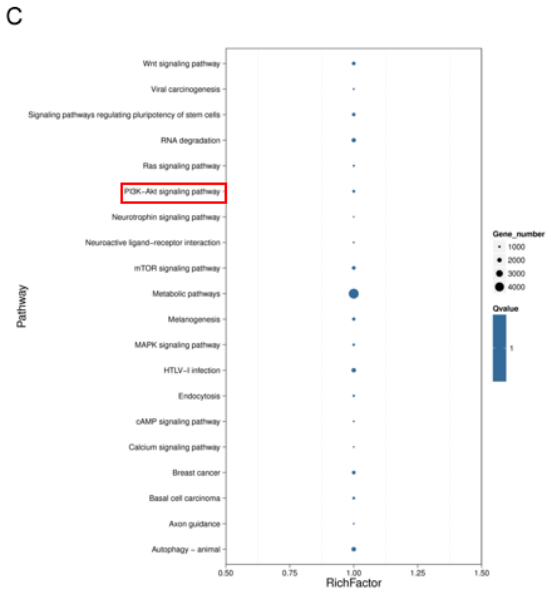


D

| miRNA | Count (AHE) | Count (ALE) | log2 Ratio(AHE/ALE) | FDR |
|---|---|---|---|---|
| hsa-miR-378b | 576 | 0 | 15.52 | 0.0000 |
| hsa-miR-1910-3p | 20 | 0 | 10.67 | 0.0000 |
| hsa-miR-21-3p | 16 | 0 | 10.36 | 0.0000 |
| hsa-miR-421 | 8 | 0 | 9.34 | 0.0019 |
| hsa-miR-221-5p | 17 | 1 | 4.31 | 0.0000 |
| hsa-miR-324-3p | 1368 | 531 | 1.65 | 0.0000 |
| hsa-miR-21-5p | 12 | 5 | 1.53 | 0.0423 |
| hsa-miR-3065-3p | 29 | 13 | 1.45 | 0.0023 |
| hsa-miR-222-3p | 21236 | 10780 | 1.26 | 0.0000 |
| hsa-miR-363-3p | 3447 | 1775 | 1.24 | 0.0000 |

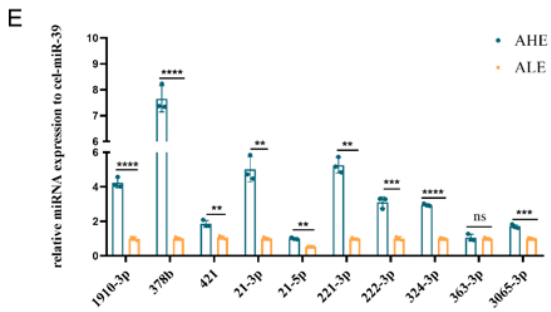


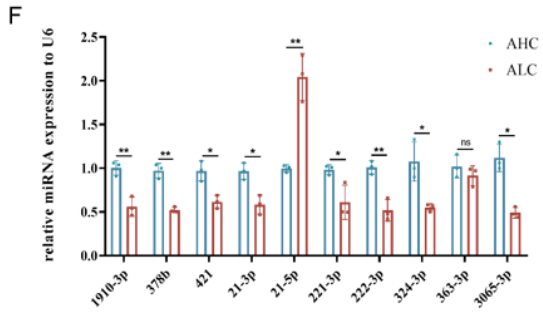

**Figure 3.** Screening and analysis of DEMs between ALE and AHE. A. Screening for differentially expressed miRNAs by comparing the expression levels between AHE and ALE. According to the FDR ≤ 0.001 and multiple differences of more than 2 times. B. The Venn diagram of targeted genes prediction for the DEMs. C. The Kyoto Encyclopedia of Genes and Genomes (KEGG) database was used to show that a total of 33 DEMs had a potential regulatory effect on the PI3K/AKT signaling pathway. D. Predicts that ten DEMs had a potential role in tumorigenesis and progression based on the reports in the literature. E, F. qRT-PCR was used to determine the differences in expression levels of ten candidate DEMs in AHE/ALE and AHC/ALC. The results showed that eight of the DEMs (miR-378b, miR-1910-3p, miR-21-3p, miR-421, miR-221-5p, miR-324-3p, miR-3065-3p, and miR-222-3p) were significantly elevated in AHE than in ALE. The data were presented as the mean ± SD. *P < 0.05, **P < 0.005, ***P < 0.001, ****P < 0.0001.

**Table 1.** The candidate miRNAs in PI3K-AKT signaling pathway

| miRNA | Count (AHE) | Count (ALE) | $log_2$ Ratio (AHE/ALE) | FDR |
|---|---|---|---|---|
| miR-378b | 576 | 0 | 15.52 | 0.0000 |
| miR-30c-1-3p | 24 | 0 | 10.94 | 0.0000 |
| miR-1910-3p | 20 | 0 | 10.67 | 0.0000 |
| miR-3653-3p | 20 | 0 | 10.67 | 0.0000 |
| miR-21-3p | 16 | 0 | 10.36 | 0.0000 |
| miR-3121-3p | 9 | 0 | 9.51 | 0.0010 |
| miR-421 | 8 | 0 | 9.34 | 0.0019 |
| miR-3684 | 5 | 0 | 8.68 | 0.0195 |
| miR-135a-3p | 4 | 0 | 8.37 | 0.0423 |
| miR-221-5p | 17 | 1 | 4.31 | 0.0000 |
| miR-141-5p | 25 | 6 | 2.35 | 0.0001 |
| miR-1254 | 405 | 99 | 2.31 | 0.0000 |
| miR-324-3p | 1368 | 531 | 1.65 | 0.0000 |
| miR-1179 | 116 | 48 | 1.55 | 0.0000 |
| miR-21-5p | 12 | 5 | 1.53 | 0.0423 |
| miR-3065-3p | 29 | 13 | 1.45 | 0.0023 |
| miR-222-3p | 21236 | 10780 | 1.26 | 0.0000 |
| miR-345-5p | 6861 | 3503 | 1.25 | 0.0000 |
| miR-363-3p | 3447 | 1775 | 1.24 | 0.0000 |
| miR-193b-3p | 9565 | 4975 | 1.23 | 0.0000 |
| miR-3124-5p | 31 | 17 | 1.15 | 0.0082 |

**Table 2.** HGSOC patients and benign patients characteristics

| Clinical parameters | |
|---|---|
| Ovarian benign patients (n = 12) Age | 59 ± 9 |
| HGSOC patients (n = 46) | 55 ± 13 |
| Ovarian cancer patients' characteristics | |
| Recurrence (%) | |
| Yes | 27 (58.7) |
| No | 19 (41.3) |
| Histology (%) | |
| Serous carcinoma | 31 (67.4) |
| Clear cell carcinoma | 6 (13.1) |
| Mucinous carcinoma | 3 (6.5) |
| Endometrioid carcinoma | 3 (6.5) |
| Unknown | 3 (6.5) |
| FIGO stage (%) | |
| I+II | 12 (26.1) |
| III+IV | 34 (73.9) |
| Lymph node (%) | |
| N0 | 15 (32.6) |
| N1 | 18 (39.1) |
| Unknown | 13 (28.3) |

lected. The average age of patients with HGSOC was 55 years. Patients with stage I+II and stage III+IV disease accounted for 26.1% (12 cases) and 73.9% (34 cases) of the cohort, respectively. Twenty-seven patients developed recurrence (58.7%). The patients' clinical pathological information is shown in **Table 2**. The expression levels of miR-1910-3p (P = 0.0017), miR-21-3p (P = 0.0037), miR-378b (P = 0.0310), and miR-421 (P = 0.0086) were significantly higher in serum exosomes derived from HGSOC patients than in those derived from benign ovarian tumor patients (**Figure 4A**; **Table 3**). The levels of miR-1910-3p, miR-421, and miR-378b were significantly higher in the serum exosomes of patients with advanced-stage disease (III+IV) than in those with early-stage disease (I+II) (P = 0.0332, P = 0.0106 and P = 0.0355, respectively; **Figure 4B**; **Table 3**). The levels of miR-421 were significantly higher in the metastatic lymph node lesions than in the primary lesions (P = 0.0399). In addition, the expression of miR-421 was significantly elevated in the recurrent lesions (P = 0.0351; **Figure 4C**; **Table 3**). Serum CA125 levels were positively correlated with the serum levels of exosomal miR-1910-3p (r = 0.454, P = 0.0003), miR-421 (r = 0.5139, P < 0.0001) and miR-378b (r = 0.3497, P = 0.0062; **Table 3**). Unfortunately, due to the short postoperative follow-up time of patients, postoperative follow-up information could not be collected. Therefore, the relationship between the candidate DEMs and patient survival and prognosis needs further study. In summary, the data indicated a

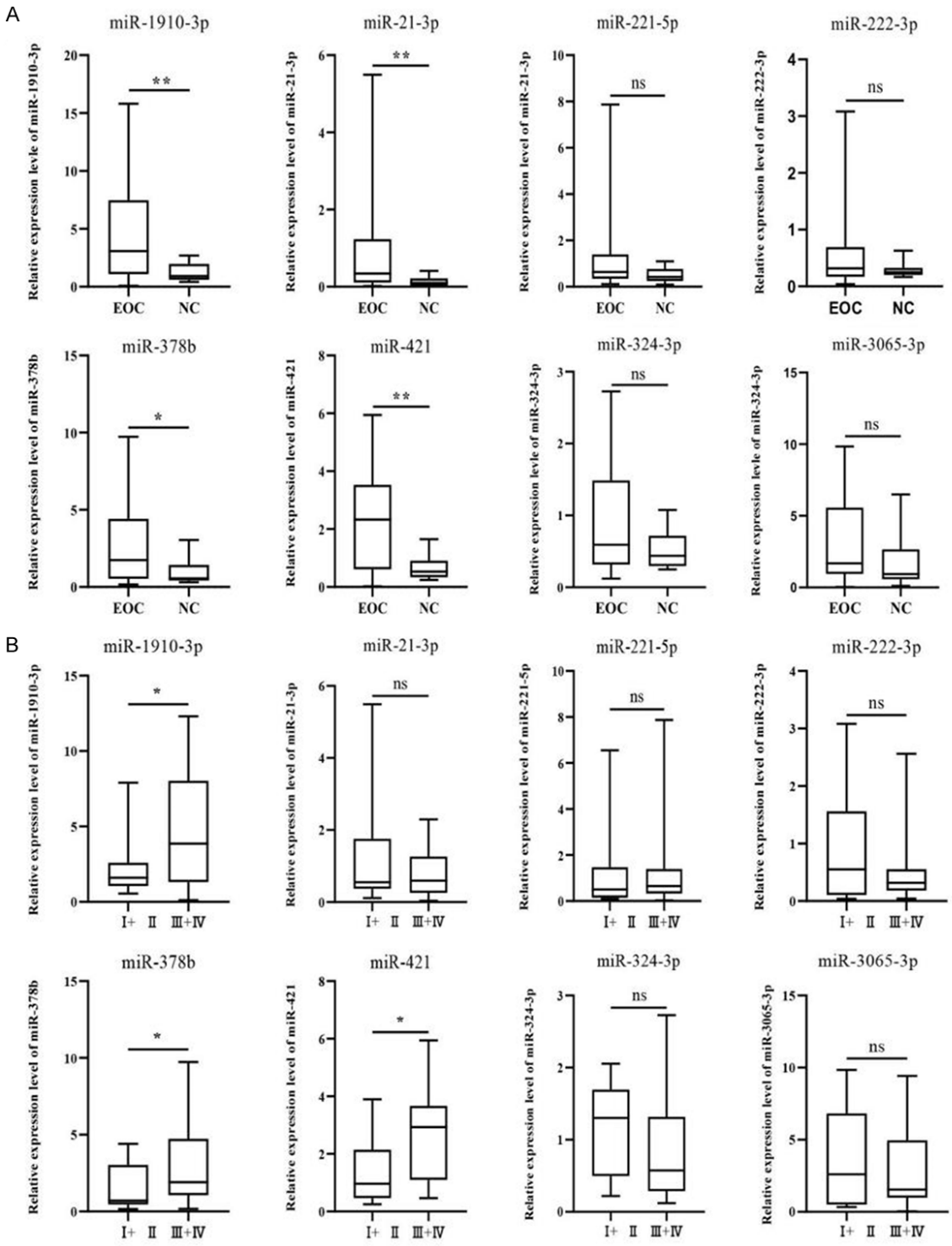
A
miR-1910-3p
Relative expression levle of miR-1910-3p
**
EOC
NC
miR-21-3p
Relative expression level of miR-21-3p
**
EOC
NC
miR-221-5p
Relative expression level of miR-21-3p
ns
EOC
NC
miR-222-3p
Relative expression level of miR-222-3p
ns
EOC
NC
miR-378b
Relative expression level of miR-378b
*
EOC
NC
miR-421
Relative expression level of miR-421
**
EOC
NC
miR-324-3p
Relative expression levle of miR-324-3p
ns
EOC
NC
miR-3065-3p
Relative expression levle of miR-324-3p
ns
EOC
NC
B
miR-1910-3p
Relative expression level of miR-1910-3p
*
I+ II III+IV
miR-21-3p
Relative expression level of miR-21-3p
ns
I+ II III+IV
miR-221-5p
Relative expression level of miR-221-5p
ns
I+ II III+IV
miR-222-3p
Relative expression level of miR-222-3p
ns
I+ II III+IV
miR-378b
Relative expression level of miR-378b
*
I+ II III+IV
miR-421
Relative expression level of miR-421
*
I+ II III+IV
miR-324-3p
Relative expression level of miR-324-3p
ns
I+ II III+IV
miR-3065-3p
Relative expression level of miR-3065-3p
ns
I+ II III+IV

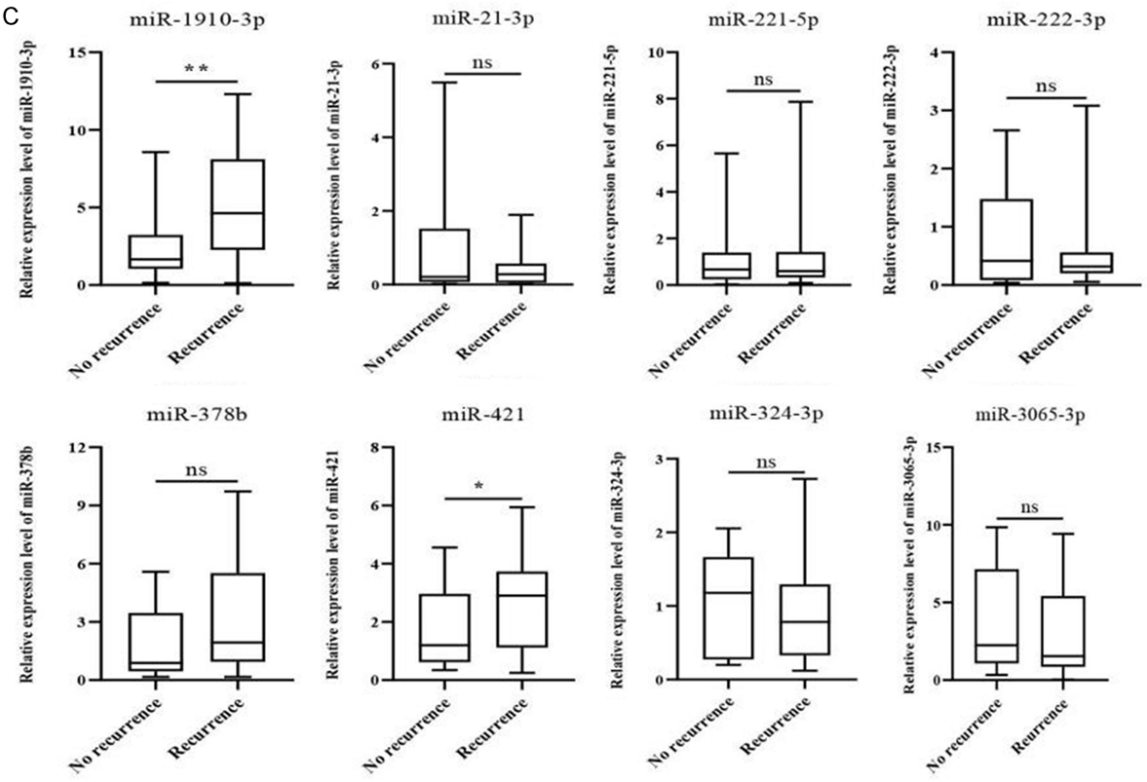


**Figure 4.** The relationship between expression levels of the candidate DEMs and clinicopathological characteristics of OC patients. A. qRT-PCR was used to determine the difference in expression levels of DEMs between HGSOC and benign patients. The expression levels of miR-1910-3p (P = 0.0017), miR-21-3p (P = 0.0037), miR-378b (P = 0.0310), and miR-421 (P = 0.0086) were significantly higher in serum exosomes derived from HGSOC patients than those derived from benign ovarian tumors patients. B, C. qRT-PCR was used to determine the relationship between DEMs and clinical staging, as well as the relationship between DEMs and recurrence. The results showed that the levels of miR-1910-3p, miR-421, and miR-378b were significantly higher in the serum exosomes of the patients with advanced-stage diseases than those with early-stage diseases (P = 0.0332, P = 0.0106 and P = 0.0355, respectively). The levels of miR-421 were significantly higher in the metastatic lymph node lesions than the primary lesions (P = 0.0399) and significantly elevated in the recurrent lesions (P = 0.0351). The data were presented as the mean ± SD. *P < 0.05, **P < 0.005, ***P < 0.001, ****P < 0.0001.

significant correlation between miR-421 and the severity and recurrence risk of HGSOC.

*Diagnostic performance of the combination of miR-1910-3p, miR-378b, and miR-421 with the tumor biomarker CA125*

The expression level of CA125 was significantly upregulated in serum exosomes of HGSOC patients vs. benign ovarian tumor patients (P < 0.005; **Figure 5A**), but the expression level was not significantly related to the patient's pathological stage (**Figure 5B**). The AUC value of serum CA125 was 0.803, and the sensitivity of serum CA125 in HGSOC diagnosis was 91.3%, yet the specificity was only 58.3%. The AUC values of miR-1910-3p, miR-378b, and miR-421 were 0.781, 0.703, and 0.851, respectively (**Figure 5C**, **5D**). The sensitivities of the exosomal levels of miR-1910-3p, miR-378b, and miR-421 in HGSOC diagnosis were 60.9%, 67.4%, and 67.4%, respectively. The specificities were 91.7%, 75.0%, and 91.7%, respectively. The AUC values of serum CA125 levels combined with miR-421, miR-1910-3p, and miR-378b were 0.877, 0.824, and 0.810, respectively. The sensitivities of serum CA125 levels in combination with miR-421, miR-1910-3p, and miR-378b in HGSOC diagnosis were 84.8%, 82.6% and 69.6, respectively. The specificities were 83.3%, 75.0% and 83.3, respectively (**Figure 5E**, **5F**). The diagnostic performance of a combination of serum CA125 and miR-421/miR-1910-3p was significantly higher than that of serum CA125 alone (P < 0.001). Moreover, the diagnostic sensitivity

**Table 3.** *P*-values of serum exosomal miRNAs in patients

| Populations | | Patient No. | | miR-1910-3p | miR-21-3p | miR-221-5p | miR-222-3p | miR-378b | miR-421 | miR-324-3p | miR-3065-3p |
|---|---|---|---|---|---|---|---|---|---|---|---|
| HGSOC vs N[a] | | 46 vs 12 | Median | 3.078 vs 0.9178 | 0.3401 vs 0.0983 | 0.6340 vs 0.4212 | 0.3169 vs 0.2479 | 1.738 vs 0.5544 | 2.330 vs 0.5296 | 0.5903 vs 0.4381 | 1.677 vs 0.9307 |
| | | | *P*-value | 0.0017 | 0.0037 | 0.0724 | 0.2558 | 0.0310 | 0.0086 | 0.1473 | 0.0730 |
| Clinical parameters in EOC patients | | | | | | | | | | | |
| Recurrence[a] | Yes | 27 | Median | 4.635 vs 1.661 | 0.2770 vs 0.2057 | 0.5959 vs 0.6721 | 0.3168 vs 0.4158 | 1.930 vs 0.88 | 2.902 vs 1.198 | 1.180 vs 0.7850 | 2.243 vs 1.547 |
| | No | 19 | *P*-value | 0.0042 | 0.5359 | 0.9296 | 0.8812 | 0.1246 | 0.1246 | 0.7740 | 0.4185 |
| FIGO stage[a] | I+II | 12 | Median | 1.604 vs 3.873 | 0.5515 vs 0.5954 | 0.5078 vs 0.6552 | 0.5501 vs 0.3168 | 0.7069 vs 1.904 | 0.9644 vs 2.932 | 1.302 vs 0.5743 | 1.547 vs 2.610 |
| | III+IV | 34 | *P*-valuec | 0.0332 | 0.4213 | 0.4213 | 0.4239 | 0.0355 | 0.0106 | 0.1157 | 0.7709 |
| LNM[a] | Yes | 15 | Median | 2.993 vs 2.026 | 0.2991 vs 0.2015 | 0.8191 vs 0.5959 | 0.3663 vs 0.3169 | 2.156 vs 1.712 | 2.932 vs 0.890 | 0.5743 vs 1.180 | 2.885 vs 1.862 |
| | No | 18 | *P*-value | 0.4860 | 0.4006 | 0.4421 | 0.9007 | 0.3247 | 0.0399 | 0.5320 | 0.3310 |
| CA125[b] | | 46 | r | 0.454 | 0.3370 | 0.3595 | 0.1543 | 0.3497 | 0.5139 | 0.3748 | 0.2151 |
| | | | *P*-value | 0.0003 | 0.0091 | 0.0048 | 0.2433 | 0.2433 | <0.0001 | 0.0034 | 0.1016 |

HGSOC: high-grade serous ovarian carcinoma; N: benign ovarian patients; FIGO: International Federation of Obstetrics and Gynecology; LNM: Lymph node metastasis; CA125: carbonhydrate antigen 125. [a]*P*-values are calculated by Mann-Whitney U test; [b]*P*-values are calculated by bivariate analyses of Spearman rho test.

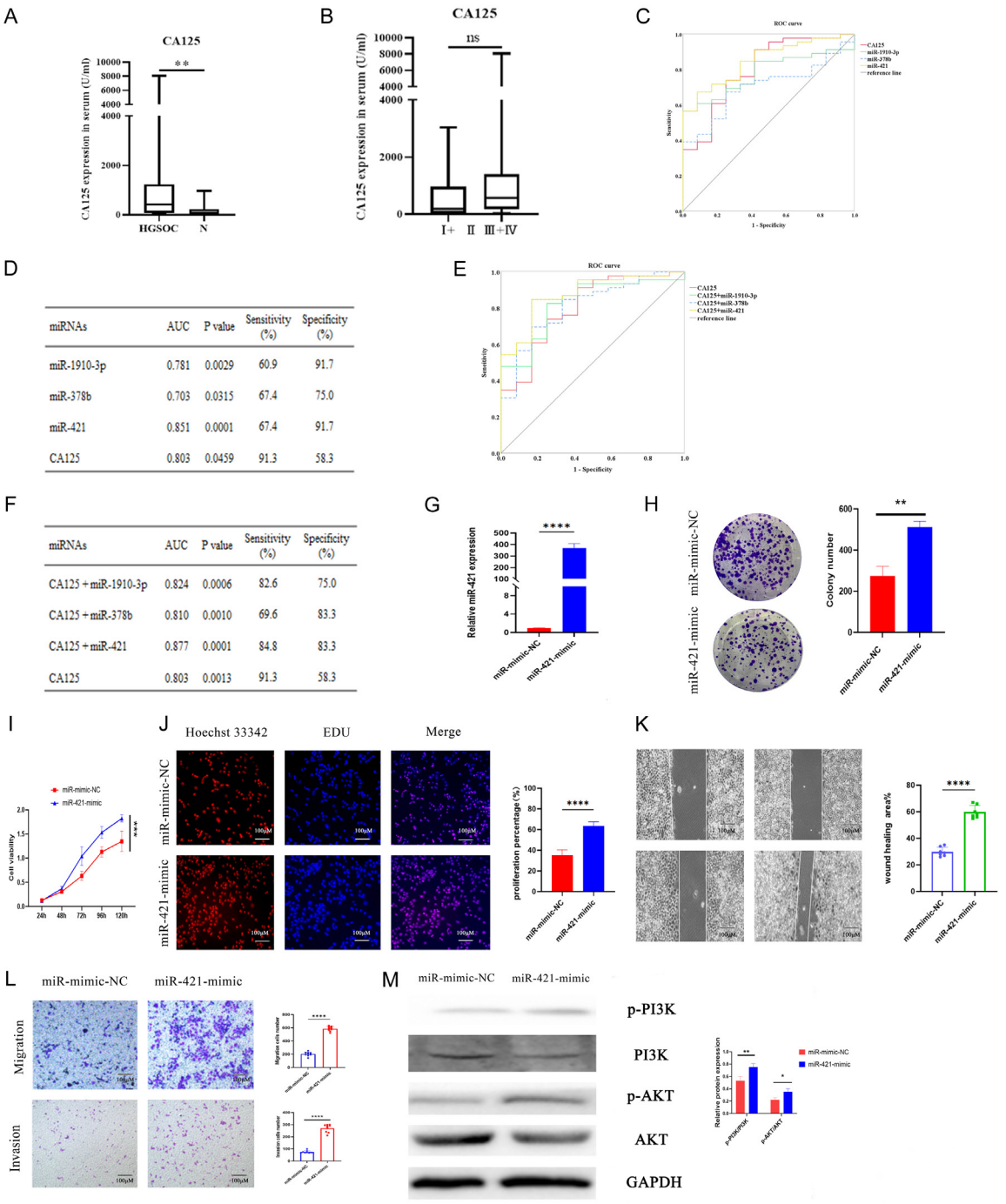


**Figure 5.** Diagnostic performance and the effect of miR-421 from exosomes on ALC. (A) The expression level of CA125 was significantly upregulated in serum exosomes of HOSGC patients. (B) The expression level of CA125 is not significantly related to clinical staging. (C) ROC curve analysis of CA125, miR-1910-3p, miR-378b, and miR-421 in the serum exosomes of HGSOC patients and benign patients. (D) The sensitivities and specificities of serum exosomal CA125, miR-1910-3p, miR-378b and miR-421. (E) ROC curve analysis of miR-1910-3p, miR-378b, and miR-421 and a combination of the CA125 in the serum exosomes of HGSOC patients and benign patients. (F) The sensitivities and specificities of miR-1910-3p, miR-378b, and miR-421 and a combination of the CA125 in the serum exosomes. (G) qRT-PCR results showed a significant upregulation of miR-421 expression in AHE after miR-421-mimic transfection. (H) Colony formation assay (274.80 ± 47.20 vs. 512.00 ± 28.15, $P < 0.005$), (I) CCK-8 assay, (J) EDU assay (63.57 ± 3.95 vs. 35.21 ± 5.45, $P < 0.0001$), (K) Wound healing assay (63.63 ± 5.15% vs. 27.52 ± 4.71%, $P < 0.0001$) and (L) Transwell Matrigel invasion/migration assay were showed that overexpression of miR-421 in AHE significantly promoted the proliferation, invasion, and migration ability of ALC compared to the

control group. (M) WB experiment showed that overexpression of miR-421 in AHE significantly activated the PI3K/AKT signaling pathway of ALC compared to the control group. The data were presented as the mean ± SD. *P < 0.05, **P < 0.005, ***P < 0.001, ****P < 0.0001. The scale bar equals 100 μm as indicated in the graph.

(84.8% vs. 82.6%) and specificity (83.3% vs. 75.0%) values of serum CA125 combined with miR-421 were higher than those of serum CA125 combined with miR-1910-3p (P < 0.001). These data suggested that the combination of miR-421 and serum CA125 is a potential ideal biomarker for the early diagnosis of HGSOC.

*The effect of miR-421 on the biological functions and activity of the PI3K/AKT pathway in ALC*

qRT-PCR showed that the expression level of miR-421 in AHE in the transfection group was significantly higher than that in AHE in the control group (P < 0.0001; **Figure 5G**). The colony formation assay (274.80 ± 47.20 vs. 512.00 ± 28.15, P < 0.005; **Figure 5H**), CCK-8 assay (P < 0.001; **Figure 5I**) and EdU assays (63.57 ± 3.95 vs. 35.21 ± 5.45, P < 0.0001; **Figure 5J**) showed that the miR-421 mimic-treated AHE (miR-421 mimic) group of ALC cells had higher proliferative activity than the mimic NC group. The wound healing assay showed that the ALC wound healing rate was significantly higher than that in the control group (63.63 ± 5.15% vs. 27.52 ± 4.71%, P < 0.0001; **Figure 5K**). The results suggested that the miR-421 mimic group had significantly enhanced migration (585.1 ± 36.27 vs. 203.0 ± 30.96, P < 0.0001; **Figure 5L**) and invasion (270.80 ± 33.20 vs. 74.56 ± 10.59, P < 0.0001; **Figure 5L**) abilities compared to the mimic NC group. WB assays showed that the protein expression levels of p-PI3K and p-AKT were significantly increased in the miR-421 mimic group (**Figure 5M**). These findings indicated that miR-421 by exosomes could enhance the malignancy of ALC by activating the PI3K/AKT pathway.

## Discussion

Exploring the potential mechanism or driving factors of ITH in OC heterogeneity is urgent. Considering the potential effect of repeated cell passaging, the distinct biological characteristics of the previously established heterogeneous cell models of OC-AHC and ALC were reconfirmed. Based on our previous work, we first explored the biological functional difference between these two cell subclones (AHC/ALC) derived from the same parent A2780 cell line in this study. The results showed that the two subclones had distinctive biological properties. AHC showed more malignant behaviors with higher migratory, invasive, and proliferative ability than ALC and more vital independent viability. Higher expression of N-cadherin and vimentin in AHC than in ALC suggests that AHC undergoes more EMT. Moreover, AHC existed excessive activation of the PI3K/AKT signaling pathway, elucidating that the PI3K/AKT signaling pathway is essential in regulating cell survival, metastasis, and proliferation. AHC cells showed more malignant behaviors than ALC cells. The results indicated that AHC/ALC cells are still ideal research models for the tumor heterogeneity of OC. In addition, the WB results confirmed our previous research findings that activation of the PI3K/AKT pathway promoted the formation of tumor heterogeneity in OC and the transformation of less invasive cell subsets into highly invasive cell subsets.

Exosomes are critical players in intercellular communication and the regulation of the TME. Recently, the role of exosomes in OC development and progression has been widely investigated [18, 19]. In our research, the exosomes were collected from the cell culture supernatant and exemplified by the TEM, NTA, and WB. The results showed that collected exosomes meet the criteria for the definition of exosomes and were performed in subsequent studies. ALC treated with AHEs showed increased proliferation, migration, and invasion abilities in comparison to treatment with PBS. The present results indicated that exosomes derived from AHC could be taken up by ALC and subsequently promote malignant behaviors of the recipient cells. In addition, the results also showed that the exosomes derived from highly malignant AHC cells can enhance the activity of the PI3K-AKT pathway in low malignant ALC cells and enhance the epithelial-mesenchymal transition ability of ALC. Exosomes play an important role in the formation of high and low-invasive cell subsets in A2780 cells. The degree of increase was positively correlated with the concentra-

tion of AHE. Nevertheless, the elevated expression of p-PI3K and p-AKT was significantly attenuated when the PI3K inhibitor LY294002 was used. These data suggested that the PI3K/AKT pathway, which induces the transformation of less aggressive cell subsets to highly aggressive cell subsets, is mediated by exosomes. In summary, the PI3K/AKT signaling pathway plays a crucial role in the occurrence and development of ovarian cancer, but the use of inhibitors of this pathway alone cannot significantly inhibit the proliferation of ovarian cancer cells, and exosomes play an important role in drug resistance in tumor treatment. Our study provides a new research approach for reducing resistance to PI3K/AKT inhibitors in cancer treatment.

Emerging evidence indicates that some exosomal miRNAs can be transferred to recipient cells to decrease the expression of target genes involved in cancer metastasis. To explore the upstream regulatory genes involved in the exosomes-mediated PI3K/AKT pathway in the formation of a heterogeneous microenvironment in OC, eight DEMs (miR-378b, miR-1910-3p, miR-21-3p, miR-421, miR-221-5p, miR-324-3p, miR-3065-3p, miR-222-3p) significantly enriched in AHE with potential regulatory effects on the PI3K/AKT pathway by bioinformatics were further identified as candidate DEMs for further analysis through quantitative transcriptome analysis of AHEs and ALEs. Among the 8 candidate DEMs, the expression of miR-421 was significantly increased in serum exosomes derived from HGSOC patients. Furthermore, miR-421 was significantly upregulated in the serum exosomes of patients with advanced and recurrent patients. MiR-421 is upregulated in many cancer cells, including gastric cancer, prostate cancer, pancreatic cancer, and non-small cell lung cancer, and predicts poor survival [20-23]. In colorectal cancer, miR-421 is upregulated in fecal samples of advanced cancer patients, and the combination of miR-421 and hemoglobin shows a higher AUC value of 0.93; The AUC for individual hemoglobin concentration is 0.67. In this study, CA125 was commonly used for the diagnosis of ovarian cancer, with an AUC of 0.803, a high sensitivity of 91.3%, but a low specificity of 58.3%, indicating its diagnostic shortcomings. However, miR-421 showed higher diagnostic ability with an AUC of 0.851, lower sensitivity at 67.4%, but higher specificity at 91.7%. The combination of miR-421 and CA125 resulted in a higher AUC of 0.877, significantly improving the specificity of CA125 in diagnosing ovarian cancer alone (83.3% vs. 58.3%) and maintaining a high sensitivity of 84.8%. Therefore, combining CA125 and miR-421 for diagnosis greatly improves the specificity and sensitivity of ovarian cancer diagnosis. This will provide new strategies for early diagnosis, detection of tumor progression trends, and the development of precision medicine.

A recent study demonstrated that overexpression of miR-421 can significantly enhance the proliferation and invasion ability of OC cells, suggesting that miR-421 plays a role as an oncogene in OC cells [24]. No research has been found on whether miR-421, mediated by exosomes, plays a role in the progression of OC. We determined that overexpression of miR-421 in AHE can significantly promote the proliferation, invasion, and migration ability of ALC cells, and activate the PI3K/AKT pathway in ALC. Our findings provide new evidence that miR-421 in exosomes promotes malignant progression of ovarian cancer cells by activation of the PI3K-AKT pathway. In addition, the results also indicated that exosomes derived from AHC can promote malignant transformation of ALC by activating the PI3K-AKT pathway, and there is a specific miRNA profile in exosomes of HGSOC and benign ovarian patients.

Importantly, miR-421 exhibits highly correlated characteristics with cancer malignancy in vitro, which can serve as a biomarker for ovarian cancer progression and a future therapeutic target for ovarian cancer. Moreover, the challenges faced in the clinical treatment of ovarian cancer mainly come from the resistance to platinum-based drugs that arise during the treatment process, many studies have shown that microRNAs play a crucial role in regulating platinum resistance. Therefore, studying the roles of miR-421 and exosomes in ovarian cancer drug resistance will be a new direction for future research.

## Conclusion

In conclusion, specific miRNAs derived from OC cells and patient serum exosomes induce the formation of a heterogeneous TME in OC. MiR-421, mediated by exosomes could induce the transformation of less invasive cell subpopula-

tions of OC cells into highly invasive cell subpopulations by activating the PI3K/AKT pathway. MiR-421 could serve as a potentially effective therapeutic target for OC. In combination with serum CA125, miR-421 might serve as a novel tumor marker for the early diagnosis of OC.

## Disclosure of conflict of interest

None.

**Address correspondence to:** Jing Wang, Beijing Key Laboratory of Mental Disorders, National Clinical Research Center for Mental Disorders and National Center for Mental Disorders, Beijing Anding Hospital, Capital Medical University, 5 Ankang Hutong, Desheng Street, Xicheng District, Beijing, China. E-mail: kycwangjing@mail.ccmu.edu.cn; Huimin Bai, Department of Gynecology, Fuxing Hospital, Capital Medical University, A20 Fuxingmenwai Street, Yuetan Street, Xicheng District, Beijing, China. E-mail: bhmdoctor@sina.com

## References

[1] Veneziani AC, Gonzalez-Ochoa E, Alqaisi H, Madariaga A, Bhat G, Rouzbahman M, Sneha S and Oza AM. Heterogeneity and treatment landscape of ovarian carcinoma. Nat Rev Clin Oncol 2023; 20: 820-842.

[2] Azzalini E, Stanta G, Canzonieri V and Bonin S. Overview of tumor heterogeneity in high-grade serous ovarian cancers. Int J Mol Sci 2023; 24: 15077.

[3] Sharma K, D'Souza RC, Tyanova S, Schaab C, Wiśniewski JR, Cox J and Mann M. Ultradeep human phosphoproteome reveals a distinct regulatory nature of Tyr and Ser/Thr-based signaling. Cell Rep 2014; 8: 1583-1594.

[4] Suh DH, Kim HS, Kim B and Song YS. Metabolic orchestration between cancer cells and tumor microenvironment as a co-evolutionary source of chemoresistance in ovarian cancer: a therapeutic implication. Biochem Pharmacol 2014; 92: 43-54.

[5] Bai H, Li H, Li W, Gui T, Yang J, Cao D and Shen K. The PI3K/AKT/mTOR pathway is a potential predictor of distinct invasive and migratory capacities in human ovarian cancer cell lines. Oncotarget 2015; 6: 25520-25532.

[6] Feng W, Dean DC, Hornicek FJ, Shi H and Duan Z. Exosomes promote pre-metastatic niche formation in ovarian cancer. Mol Cancer 2019; 18: 124.

[7] Lee W, Ko SY, Mohamed MS, Kenny HA, Lengyel E and Naora H. Neutrophils facilitate ovarian cancer premetastatic niche formation in the omentum. J Exp Med 2019; 216: 176-194.

[8] Zhou W, Ma J, Zhao H, Wang Q, Guo X, Chen L, Cao Z, Xu J, Zhang B and Zhou X. Serum exosomes from epithelial ovarian cancer patients contain LRP1, which promotes the migration of epithelial ovarian cancer cell. Mol Cell Proteomics 2023; 22: 100520.

[9] Sepúlveda F, Mayorga-Lobos C, Guzmán K, Durán-Jara E and Lobos-González L. EV-miRNA-mediated Intercellular communication in the breast tumor microenvironment. Int J Mol Sci 2023; 24: 13085.

[10] Suzuki HI, Katsura A, Matsuyama H and Miyazono K. MicroRNA regulons in tumor microenvironment. Oncogene 2015; 34: 3085-3094.

[11] Cui R, Cao G, Bai H and Zhang Z. LPAR1 regulates the development of intratumoral heterogeneity in ovarian serous cystadenocarcinoma by activating the PI3K/AKT signaling pathway. Cancer Cell Int 2019; 19: 201.

[12] Bai H, Li H, Li W, Gui T, Yang J, Cao D and Shen K. The PI3K/AKT/mTOR pathway is a potential predictor of distinct invasive and migratory capacities in human ovarian cancer cell lines. Oncotarget 2015; 6: 25520-32.

[13] Au Yeung CL, Co NN, Tsuruga T, Yeung TL, Kwan SY, Leung CS, Li Y, Lu ES, Kwan K, Wong KK, Schmandt R, Lu KH and Mok SC. Exosomal transfer of stroma-derived miR21 confers paclitaxel resistance in ovarian cancer cells through targeting APAF1. Nat Commun 2016; 7: 11150.

[14] Morelli AE, Larregina AT, Shufesky WJ, Sullivan ML, Stolz DB, Papworth GD, Zahorchak AF, Logar AJ, Wang Z, Watkins SC, Falo LD Jr and Thomson AW. Endocytosis, intracellular sorting, and processing of exosomes by dendritic cells. Blood 2004; 104: 3257-3266.

[15] Jiao R, Sun S, Gao X, Cui R, Cao G, Wei H, Wang S, Zhang Z and Bai H. A polyethylene glycol-based method for enrichment of extracellular vesicles from culture supernatant of human ovarian cancer cell line A2780 and body fluids of high-grade serous carcinoma patients. Cancer Manag Res 2020; 12: 6291-6301.

[16] Wang S, Song X, Wang K, Zheng B, Lin Q, Yu M, Xie L, Chen L and Song X. Plasma exosomal miR-320d, miR-4479, and miR-6763-5p as diagnostic biomarkers in epithelial ovarian cancer. Front Oncol 2022; 12: 986343.

[17] Krijgsveld J, Gauci S, Dormeyer W and Heck AJ. In-gel isoelectric focusing of peptides as a tool for improved protein identification. J Proteome Res 2006; 5: 1721-1730.

[18] Nakamura K, Sawada K, Kobayashi M, Miyamoto M, Shimizu A, Yamamoto M, Kinose Y and Kimura T. Role of the exosome in ovarian cancer progression and its potential as a ther-

apeutic target. Cancers (Basel) 2019; 11: 1147.
[19] Kim H, Lee S, Shin E, Seong KM, Jin YW, Youn H and Youn B. The emerging roles of exosomes as EMT regulators in cancer. Cells 2020; 9: 861.
[20] Ma J, Zhao G, Du J, Li J, Lin G and Zhang J. LncRNA FENDRR inhibits gastric cancer cell proliferation and invasion via the miR-421/SIRT3/Notch-1 axis. Cancer Manag Res 2021; 13: 9175-9187.
[21] Yin Y, Xu L, Chang Y, Zeng T, Chen X, Wang A, Groth J, Foo WC, Liang C, Hu H and Huang J. N-Myc promotes therapeutic resistance development of neuroendocrine prostate cancer by differentially regulating miR-421/ATM pathway. Mol Cancer 2019; 18: 11.
[22] Shopit A, Li X, Tang Z, Awsh M, Shobet L, Niu M, Wang H, Mousa H, Alshwmi M, Tesfaldet T, Gamallat Y, Li H, Chu P, Ahmad N, Jamalat Y, Ai J, Qaed E, Almoiliqy M, Wang S and Tang Z. miR-421 up-regulation by the oleanolic acid derivative K73-03 regulates epigenetically SPINK1 transcription in pancreatic cancer cells leading to metabolic changes and enhanced apoptosis. Pharmacol Res 2020; 161: 105130.
[23] Duan FG, Wang MF, Cao YB, Dan Li, Li RZ, Fan XX, Khan I, Lai HL, Zhang YZ, Hsiao WW, Yao XJ, Wu QB, Liu L, Tang YJ and Leung EL. MicroRNA-421 confers paclitaxel resistance by binding to the KEAP1 3'UTR and predicts poor survival in non-small cell lung cancer. Cell Death Dis 2019; 10: 821.
[24] Wang Z, Zhang W, Fang J, Xie P, Miao M and Yang H. Circular RNA circEXOC6B inhibits the progression of ovarian cancer by sponging miR-421 and regulating RUS1 expression. Onco Targets Ther 2020; 13: 8233-8243.

**Table S1.** The total miRNAs in PI3K-AKT signaling pathway

| miRNA id | Count (AHE) | Count (ALE) | $\log_2$ Ratio (AHE/ALE) | FDR |
|---|---|---|---|---|
| miR-378b | 576 | 0 | 15.52 | 0.0000 |
| miR-30c-1-3p | 24 | 0 | 10.94 | 0.0000 |
| miR-1910-3p | 20 | 0 | 10.67 | 0.0000 |
| miR-3653-3p | 20 | 0 | 10.67 | 0.0000 |
| miR-21-3p | 16 | 0 | 10.36 | 0.0000 |
| miR-3121-3p | 9 | 0 | 9.51 | 0.0010 |
| miR-421 | 8 | 0 | 9.34 | 0.0019 |
| miR-3684 | 5 | 0 | 8.68 | 0.0195 |
| miR-135a-3p | 4 | 0 | 8.37 | 0.0423 |
| miR-221-5p | 17 | 1 | 4.31 | 0.0000 |
| miR-141-5p | 25 | 6 | 2.35 | 0.0001 |
| miR-1254 | 405 | 99 | 2.31 | 0.0000 |
| miR-324-3p | 1368 | 531 | 1.65 | 0.0000 |
| miR-103a-2-5p | 116 | 48 | 1.55 | 0.0000 |
| miR-21-5p | 12 | 5 | 1.53 | 0.0423 |
| miR-3065-3p | 29 | 13 | 1.45 | 0.0023 |
| miR-222-3p | 21236 | 10780 | 1.26 | 0.0000 |
| miR-345-5p | 6861 | 3503 | 1.25 | 0.0000 |
| miR-363-3p | 3447 | 1775 | 1.24 | 0.0000 |
| miR-193b-3p | 9565 | 4975 | 1.23 | 0.0000 |
| miR-3124-5 | 31 | 17 | 1.15 | 0.0082 |
| miR-219a-1-3p | 91 | 57 | 0.96 | 0.0001 |
| hsa-let-7c-5p | 47754 | 31007 | 0.91 | 0.0000 |
| miR-16-2-3p | 75 | 49 | 0.90 | 0.0008 |
| miR-23b-5p | 853 | 583 | 0.83 | 0.0000 |
| miR-200c-3p | 1394 | 1073 | 0.66 | 0.0000 |
| miR-33b-3p | 107 | 95 | 0.45 | 0.0286 |
| hsa-let-7f-5p | 250961 | 223958 | 0.45 | 0.0000 |
| miR-218-5p | 29711 | 26626 | 0.44 | 0.0000 |
| miR-378a-5p | 286 | 260 | 0.42 | 0.0009 |
| miR-183-5p | 30478 | 30256 | 0.29 | 0.0000 |
| miR-1179 | 1790 | 1951 | 0.16 | 0.0011 |
| miR-361-3p | 243371 | 275353 | 0.11 | 0.0000 |

FDR: false discovery rates. The criteria for screening is FDR ≤ 0.001 and a fold change of more than 2.